Blaisonneau *et al. Geotherm Energy (2016) 4:3*
DOI 10.1186/s40517-016-0045-9

Geothermal Energy
a SpringerOpen Journal

RESEARCH Open Access

Evolution of fracture permeability with respect to fluid/rock interactions under thermohydromechanical conditions: development of experimental reactive percolation tests

A. Blaisonneau*, M. Peter-Borie and S. Gentier

*Correspondence:
a.blaisonneau@brgm.fr
Georesources Division,
Geothermal Energy
Department, BRGM,
3 Avenue Claude Guillemin,
BP 6009, 45060 Orleans
Cedex 2, France

Abstract

The evolution of fracture permeability is crucial as regards the lifespan of the deep fractured geothermal exchanger of an Enhanced Geothermal System site. The objective in developing reactive percolation tests in fractures under thermohydromechanical conditions is to improve our understanding of fluid/rock interactions and their role in the evolution of fracture permeability. This article describes the test apparatus and the experimental protocol developed to meet this objective. The data from a test on a sample of fractured granite are interpreted with a view to characterising the phenomena that occurred during the reactive percolation and their impact on the behaviour of the fracture and its permeability. The test showed that the *free face type dissolution* of some minerals led, through a deepening of existing channels on the fracture walls, to an increase of the fracture's permeability by one order of magnitude and to a change in its hydromechanical behaviour.

Keywords: Fracture, Permeability, Fluid/rock interactions, Laboratory testing, Fracture characterisation, Engineered/Enhanced Geothermal System (EGS)

Background

The need to diversify the energy mix has, among other things, led to attempts to generalise the use of the Earth's heat for the production of heat and/or electricity. Moving beyond the "classic" geothermal energy stage associated with active volcanic areas and specific aquifers whose hydraulic and thermal characteristics are directly and economically exploitable is a new field of geothermal energy known as the Engineered/Enhanced Geothermal Systems (EGS). These systems use deep underground (high-temperature) rock formations as heat exchangers through promoting the circulation of a natural fluid (MIT 2006). In the absence of a typical aquifer (permeable porous medium), natural fluids circulate in complex hydraulic systems made up of fracture and fault networks that are more or less well connected, depending on the considered scale. The aim of the new exploitation techniques is to provoke fluid circulation between an injection

well and one or more production wells, thus modifying the local circulation dynamics in order to obtain an economically viable flow rate and temperature. Given their weak injectivity and initial productivity, the wells in these environments commonly require a development phase based on hydraulic and/or chemical stimulation through overpressurised injection of a cold fluid into the hot fractured medium. During this development phase, predominant physical processes in the fracture network depend on the stimulation scenario: hydromechanical processes are of first order during hydraulic stimulation, whereas hydrochemical processes drive the behaviour during chemical stimulation. Following the development phase, the cost effectiveness of these systems lies in their sustainability over time, i.e. at least 20 years of operation without any substantial reduction in well injectivity and/or productivity or any thermal short circuit due to a localised increase in the permeability of the deep fractured rock mass. During this exploitation phase of the EGS, the problem of permeability evolution in a natural fracture (basic element of the hydraulic system in question) due to fluid–rock interactions, within a varying thermal and mechanical context depending on the distance from the well, is a crucial issue.

For over 20 years, the Soultz-sous-Forêts experimental site in Alsace (France) has been dedicated to the scientific study of these new geothermal systems (Genter et al. 2010). The various research projects carried out at this site have shown the importance of understanding both the natural and the induced circulation of fluids in the fractured and/or faulted granitic basement and its evolution in situations of specific thermal and mechanical stress. This problem, which is relatively new in the field of geothermal energy, is similar to that posed over the past 30 years in connection with the underground storage of radioactive waste (Rutqvist and Stephansson 2003) and more recently in the oil industry for the exploitation of fractured reservoirs.

The evolution of a fracture's hydraulic behaviour under both normal stress and shear has already been widely studied in relation to the storage of nuclear waste in the 1980s and 1990s. The experimental studies resulted in the relationship between hydromechanical behaviour and fracture morphology being taken into account more or less explicitly and in more or less detail. The morphology of the walls and their degree of match, quantified through various approaches, has proved to be an important parameter as regards both normal stress (evolution of the contact surfaces with increasing stress) and shear (evolution of the friction surfaces according to their "angularity"). Over and above understanding the mechanical behaviour, the evolution of the fracture morphology determines the evolution of its permeability in expressing the deformation of the hydraulically effective volumes. Conversely, the thermomechanical behaviour of fractures has been little studied and remains a completely open and critical issue for understanding phenomena in the EGS context, independently of the thermal stimuli themselves.

The evolution of a fracture's permeability as a result of fluid–rock interaction is an even more recent problem and is still little studied from either the experimental or the modelling standpoints. Although coupled models are beginning to be developed from a theoretical or empirical point of view, their validation is far from being realized, notably due to the lack of a sufficient number of adequately instrumented laboratory experiments to take into account the different interfering hydraulic, mechanical and thermal aspects. This validation requires, among other things, an understanding of the chemical

phenomena occurring within the fracture and the changes in the fracture's morphology. A number of recent studies (Polak et al. 2003; Yasuhara et al. 2006; McGuire et al. 2013; Zhao et al. 2014) are devoted to chemical interactions in fractures and, in particular, to the different types of mineral dissolution patterns. Two types of dissolution phenomena are identified: those of the *free face dissolution* type and those of the *pressure solution* type. The latter correspond to chemical corrosion of the fracture asperities in contact resulting from the localised concentration of pressure at these points leading to greater mineral solubility (Zhao et al. 2014). The dominance of this *pressure solution* effect is notably due to mechanical loading and the effective pressure applied to the fracture (McGuire et al. 2013). The two types of dissolution phenomena may impact differently on the hydraulic behaviour and permeability of the fracture: the channelling effects induced by *free face dissolution* and giving rise to increase in the fracture's permeability can be offset by the chemical attack on the fracture asperities in contact which, conversely, brings about a decrease in the hydraulic opening and thus the permeability (Polak et al. 2003). When the fracture is at the same time submitted to a normal stress, a mechanical closure is superimposed to these closures/apertures due to chemical phenomena. Several relevant processes can explain the mechanical closure of a fracture under normal stress. Indeed, in addition to its elastic part, an irreversible closure of the fracture can occur due to mechanisms such as *damage* by brittle fractures or plastic flow of contacts (Brown and Scholz 1986), *viscous creep* of the contacts inducing time-dependent closure (Matsuki et al. 2001) or *stress corrosion* process (Yasuhara and Elsworth 2008). This latter process induces a compaction of the fracture by combining mechanical and chemical phenomena: the tensile stresses resulting from the compressive loading of contacting asperities induce "subcritical" or "quasistatic" cracking in the matrix around them and the presence of fluid can lead to a growth of these fractures due to chemical reactions. In addition to these processes, when the fracture is submitted to temperature, a thermal over-closure can occur (Barton and Makurat 2006). All these processes can superimpose and the predominance of one or another will depend on the loading conditions (level of normal stress, temperature), the type of rock, the fluid composition and the morphology of the fracture. As far as the latter is concerned, numerous experimental works are carried out with "artificial" in lab-made fractures. Depending on the way they are created, such "fresh" fractures will be free of coating and mineral deposits on their wall and their asperities will have a high angularity. When the fracture is submitted to a normal stress, this point can increase the stress concentration and then intensify the irreversible mechanisms such as damage, stress corrosion and pressure solution. In contrast, natural fractures can exhibit coating due to their history—fluid circulation or chemical phenomena—and their asperities can be rounded, which can limit stress concentrations.

Using experience gained from laboratory studies of a fracture's hydromechanical behaviour under normal stress and preliminary developments for studying the effect of acidification under controlled temperature, we built and gradually improved an experimental apparatus so as to provide a percolation cell in a fracture under imposed stress and temperature conditions (Gentier et al. 1998). This apparatus, after various stages of adaptation and experimental validation, enables us to study the complex physical phenomena that can play a fundamental role in the success of EGS.

In addition to describing the experimental apparatus and the first results obtained on the evolution of fracture permeability, we aim to highlight the need for a strict upstream experimental protocol for the reactive percolation so as to enable meaningful interpretation of the results. The work presented here was carried out on a natural fracture in a core obtained from a depth of 1890 m in drill-hole EPS1 at Soultz-sous-Forêts.

Methods

The aim of the in-fracture reactive percolation tests under an imposed normal stress and temperature is to characterise the evolution of the fracture's hydraulic and hydromechanical behaviour with, in the first instance, the evolution of its permeability induced by the fluid/rock interactions resulting from the injection of an imposed chemical fluid. To achieve this aim, the work carried out over the last 10 years has been focused on developing the experimental apparatus and on establishing a methodology for obtaining the necessary data and information through a series of tests and characterisations carried out before and after the reactive percolation test itself.

Principle of the tests and experimental apparatus

The tests are performed on cylindrical samples of fractured rock cored such that the mean plane of the fracture is perpendicular to the cylinder's axis of symmetry. The principle of the tests is to percolate a fluid through a natural fracture contained in a rock sample, under imposed and/or controlled THM conditions. The fluid, of known and constant chemical composition (the percolated fluid not being recycled), is injected into the centre of the fracture by boring into the lower wall, resulting in a divergent radial flow within the fracture. The evolution of the fluid's chemical composition is then characterised after passage through the fracture. The tests were performed within a containment cell at an imposed temperature and with a normal stress loading on the sample perpendicular to the fracture plane.

The experimental apparatus is shown schematically in Fig. 1:

- The hydraulic part of the test consists in injecting the fluid at a prescribed flow rate with a chromatography pump, which also measures the injection pressure. Once the fluid has percolated through the fracture, it is recovered in an annular reservoir surrounding the rock sample. With the containment cell being pressurised (0.1 MPa), each time the solenoid valves located outside the chamber (at atmospheric pressure) are opened, the pressure difference flushes the fluid from the annular reservoir via capillaries (with a diameter of 1/16th of an inch) to the systems for measuring the physicochemical changes in the fluid, for collecting samples and for monitoring the outflow. The last, which is done by weighing the fluid, enables one to verify, for an imposed injection rate, that there is no fluid loss in the circuit whether through leakage or excessive evaporation. To limit evaporation, the nitrogen used for pressurising the cell is water saturated through bubbling.
- For mechanically monitoring the tests, a force-controlled press is used to apply a force in the axis of the cylindrical sample and thus load the fracture under normal stress. Four displacement sensors distributed around the sample measure the relative displacements of the walls. These measurements include both the deformation of the

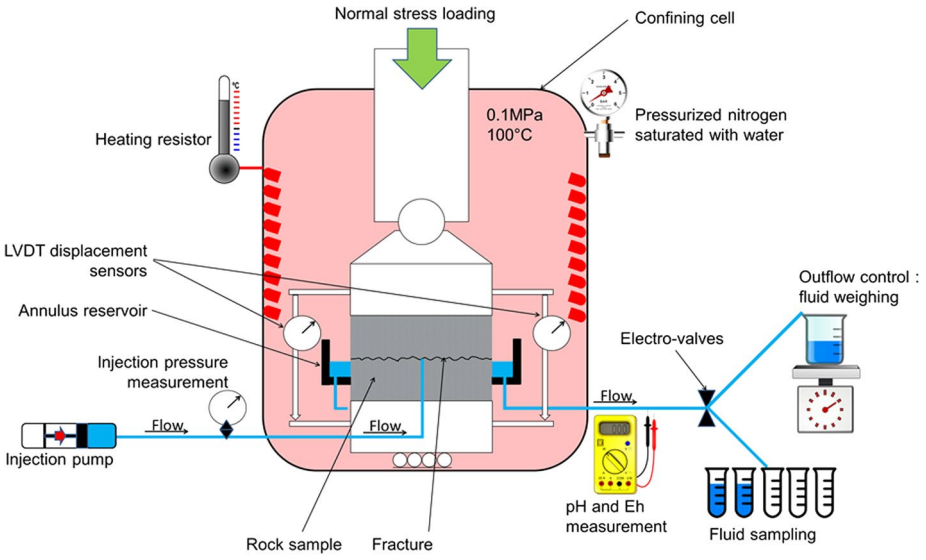

Fig. 1 Diagram of the experimental apparatus

walls and the closing/opening of the fracture; however, for rocks whose matrix can be considered as poorly deformable in terms of the applied normal stress level, these measurements provide direct access to the opening or closure of the fracture. This has to be checked considering the Young's modulus of the rock matrix and the level of normal stress applied.

- For thermally monitoring the tests, a temperature-controlled heating resistor installed on the wall of the containment cell enables one to regulate the cell temperature. The apparatus does not guarantee a uniform temperature within the containment cell, which is why the temperature is measured at various points using PT100 probes distributed over the height of the cell (bottom, middle and top), and using thermocouples for measurements at the rock sample and fluid contacts (i.e. at the point of injection into the fracture, at the contact with the fluid in the annular reservoir and at the level of the upper wall rock matrix).
- For monitoring the physicochemical evolution of the fluid, the experimental apparatus enables both online monitoring of certain of the fluid's parameters after its passage through the fracture and sampling of the fluid in order to perform targeted analyses of the chemical elements required for monitoring changes in the fluid's chemical composition (the chemical composition of the injected fluid being known). The fluid's pH and Eh are measured online using pH/Eh sensors at the exit of the containment cell, thus enabling the reactivity of chemical processes to be checked. The sampling is done by an automatic fraction collector that extracts the fluid volumes required for analyses undertaken in suitable packaging (open tubes, vacuum-sealed tubes) and according to a sampling frequency adapted to the test's reactivity.

Methodology

To assess the fluid/rock interactions and their influence on the evolution of the fracture's permeability, we developed a methodology associated with the operation of the

experimental apparatus. It is based on a set of morphological, petrographic, chemical and physical characterisations and on hydromechanical behavioural tests under normal stress and temperature (summarised in Fig. 2) carried out before and after the reactive percolation test.

To determine the fracture's petrographic, physical, chemical and morphological characteristics, we

- analysed and described the minerals on the fracture walls and in the rock matrix;
- mapped the fracture's voids (Gentier and Billaux 1989) by analysing images of the void casts;
- mapped the topography of the fracture walls by profiling with a laser profilometer; and
- mapped the chemical elements of the fracture walls using X-ray microfluorescence.

The compositions of the fluids used during the characterisation phases of the fracture's hydromechanical behaviour are determined after the characterisations and before the reactive percolation test (Fig. 2). Moreover, to avoid any fluid/rock interactions during these phases, the fluids are determined so as to be chemically inert with respect to the sample's minerals, whether in the matrix or on the fracture walls.

Once the sample is placed in the experimental apparatus, a loading protocol is applied so as to rematch the fracture walls. The protocol consists in carrying out cycles of mechanical loading/unloading followed by a hydraulic test. At the end of each loading/unloading cycle, the mean residual irreversible displacement due to the cycle is determined from the LVDT displacement sensors. The mechanical criterion of the rematch is when the mean irreversible displacement after a cycle tends to zero. For the hydraulic test, a given flow rate is imposed following a mechanical cycle and the injection pressure

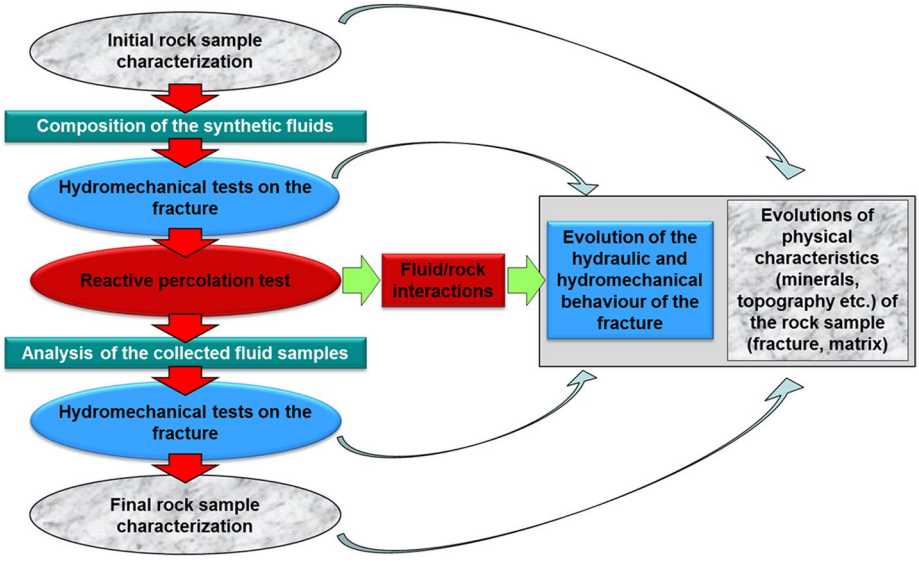

Fig. 2 Methodology of the percolation tests. The *red arrows* indicate the chronological sequence, the *green* ones mean "induce" and the *thin grey* ones indicate which data or characteristics are compared in order to determine the evolutions referenced on the *right*

is measured. The hydraulic criterion of the rematch is when the pressure given by two successive hydraulic tests is constant. The fracture's rematch is considered effective when both the mechanical and hydraulic criteria have been achieved. Once the fracture has been rematched, and to ensure this state throughout the test, a minimum normal stress, termed pre-load stress, is applied continuously to the sample. In order to avoid/limit any mechanical damage of the asperities in contact during the rematching, the maximum value of normal stress applied will be determined by considering the in situ normal stress submitted by the fracture.

The mechanical, hydraulic and hydromechanical behaviour of the fracture is characterised through injection tests. By injecting chemically inert fluids at different rates under several normal stress levels, one can characterise the fracture's closing/opening and the evolution of injection pressure versus flow, and also estimate the flow regime within the fracture.

Acquisition of the fracture's morphological features

The mechanical behaviour and flow properties of fractures depend largely on the surface roughness of their walls and their match (Barton and Choubey 1977; Gentier et al. 2000; Crandall et al. 2010): the walls of natural fractures are surfaces with ripples of different wavelengths that can be as much as the asperities directly associated with the minerals or component elements. In particular, Hopkins (2000) highlighted the determining role of the contact zone characteristics (shape, size, number, distribution and resistance) on the fracture's mechanical properties and of the structure of the free space between the walls (void space) on the hydraulic properties.

To quantify the potential changes in the void space and contact zones following a reactive percolation, the roughness at sample scale is depicted by topographic maps of the two fracture walls and by a thickness/height map of the voids. The combination of the three maps enables the fracture morphology to be characterised by magnitudes derived from statistical and geostatistical calculations. To enable both a spatial repositioning and a superpositioning of these maps, three cylindrical Teflon inserts, one millimetre in diameter, are embedded in each of the walls, with spatial correspondence of the points once the two walls have been rematched. The inserts are unique points, both chemically and topographically, that are easily identifiable on the different maps.

Mapping the wall topography

The most classic methods for analysing fracture surface topography are based on topographic profiles (mechanical [sensor or needle] profilographs, optical profilographs [such as light section microscopy], interferometry, speckle metrology and laser profilometry; Maerz et al. 1990; Ge et al. 2014). These methods enable relatively standard "roughness" parameters to be estimated through statistical analyses or comparisons with type profiles. The study necessary for an in-depth understanding of the interaction phenomena, which may be local, requires a more precise and detailed 3D approach. For this, the surfaces can be reconstructed from linear recordings (profiles) through geostatistical treatment (Chilès and Gentier 1993), with the quality and precision depending on the density of recorded information. Other optical methods (methods based on structured light projection techniques: laser scanning and stereo topometric cameras) now enable

three-dimensional surfaces to be obtained directly (Ge et al. 2014.). This type of method, giving a high-resolution map of the entire surface, was used for studying the topography of the wall surfaces of our granite sample. A laser scan of the walls was done using a laser profilometer (NanoFocus AG laser profilometer with ©NanoFocus µscan35 software; Fig. 3a). To study the differences in wall topography before and after the percolation test, the walls were fixed in a support enabling their identical repositioning before and after the percolation test so as to minimize the map rotations and translations necessary for a good superposition. This method provided a map with a lateral resolution of 25 µm (Figs. 3b, c1), a vertical error estimated at 10 µm and a horizontal error estimated at 25 µm.

Mapping the void thicknesses (or heights)

Estimating the thickness (or height) of the voids left after matching the walls is difficult. Recalibrating the topographic data acquired on each of the walls is problematic due to the thickness of the very small voids compared to the different undulations and irregularities of each wall. From a mechanical standpoint, some authors have limited themselves to estimating the contact zones: area and distribution. Among these methods are those based on the distribution of temperatures using thermocouples (Teufel and Logan 1978), on resistance to the passage of an electric current from one wall to the other (Power and Hencher 1996) and on the impression of the contact zones obtained with pressure-sensitive paper (Duncan and Hancock 1966) or deformable film (Iwai 1976; Bandis et al. 1983). Methods of injecting the fracture using a metal alloy with a low melting point, such as Wood's metal (Pyrak-Nolte et al. 1987; Yasuhara et al. 2006), also restrict the information obtained to binary data: injectable or contact zone. Furthermore, it does not enable reuse of the fracture after injection.

From a hydraulic standpoint, knowledge of the zones in contact and otherwise is not really sufficient because the potential interactions that can affect the contacts can

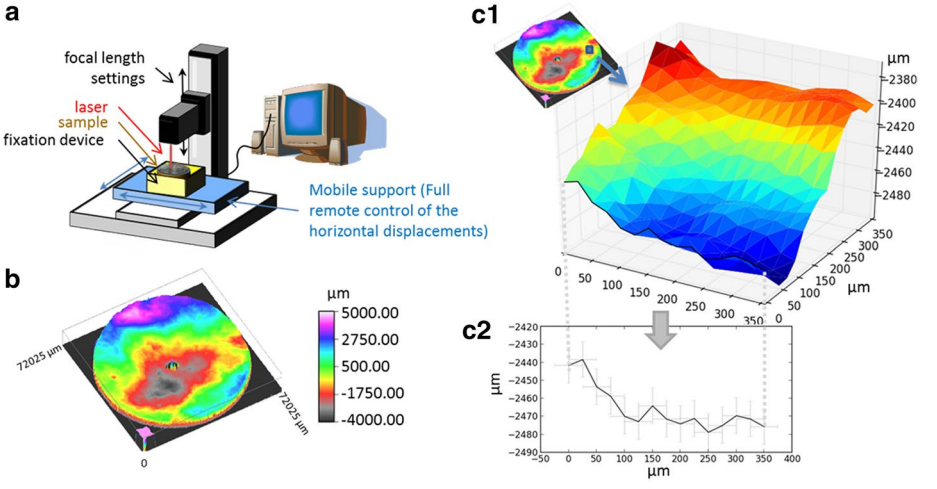

Fig. 3 Mapping of the wall topography. **a** Measuring apparatus; **b** raw topographic map of the lower wall in its support; **c1** detail of the lower wall topography; **c2** example of a profile of the **c1** detail with associated *error bars*

also modify the existing voids. The morphology of the void space can be obtained (1) through X-ray tomography as used by Keller (1998) and Re and Scavia (1999), although this does not allow the detection of voids less than 0.5 mm thick, (2) through injecting a coloured Epoxy-type resin (Gale 1987), which involves destruction of the sample, or (3) through injecting a soft coloured resin (Gentier et al. 1989) allowing the mould to be removed cleanly from the fracture, which is then reusable. The last method, which was used in this study, enables multiple casts on the same sample and, more specifically, both before and after the reactive percolation. Moulding the voids is done by expulsing the coloured silicon resin from the fracture previously filled with the fluid resin when adjusting the two walls. The resin's colour is adapted to the range of the fracture's widths; the thicker the mould, and thus the thicker the void, the darker the resin. At the same time, a calibration wedge with a bilinear thickness variation is moulded with the same resin preparation for calibrating the relationship between colour and thickness (Fig. 4). Images of the void moulds and the associated calibration wedge are obtained by light transmission using the same protocol; the resulting images are 16-bit coded RGB images (that is 65 536 or 256^2 unique values for each red, green and blue component) in which each pixel corresponds to a square of 35 μm sides, providing a horizontal resolution of the same order of magnitude as the topographic maps of the walls (25 μm). The images are corrected for non-uniformity of the light source so as to eliminate any bias in capturing the transmission images. The image of the calibration wedge is then analysed in order to assign a thickness to each grey-scale value, coded on 256^2 unique values, based on which the image of the void moulds is transformed into a void thickness map (Fig. 5). Studying the dispersion of the grey levels for each void thickness against the image of the corrected calibration wedge mould made it possible to estimate the thickness error as ±10 μm, which is identical to that of the topographic maps of the walls.

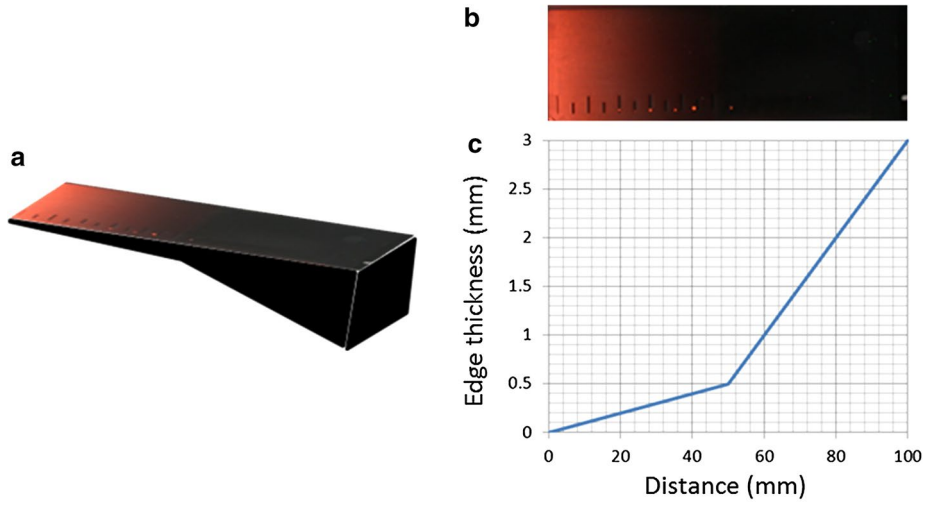

Fig. 4 Calibration between colour and thickness. **a** View of the calibration wedge (*exaggerated thickness*); **b** plan view of the calibration wedge; **c** theoretical curve giving the thickness of the calibration wedge according to distance from the wedge's first graduation

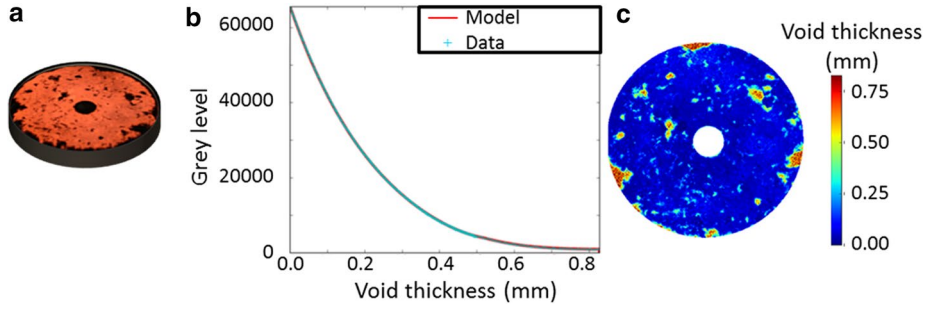

Fig. 5 Mapping of the void thicknesses. **a** View of a void mould (*exaggerated thickness*); **b** curve for calibrating void thickness from the *grey* levels in the calibration wedge and void mould images; **c** map of the void thicknesses before the percolation test

Rotating the void thickness maps made it possible to superpose them and study the differences before and after the percolation test, as well as to align them with the topographic maps of the walls based on the position of the reference pins.

Results: test on a granite sample

Initial characterisation of the rock sample

The granite sample containing the natural fracture was taken from a core obtained at a depth of 1890 m in drill-hole EPS1 at the Soultz-sous-Forêts site (France). By assuming that the in situ vertical stress is given by Eq. 1 (Cornet et al. 2007) and that in situ the fracture was sub-horizontal (drilling-hole vertical and fracture slightly perpendicular to the drilling core), we can estimate that the in situ normal stress acting on the fracture was approximately 46 MPa. Based on this value, in order to limit any mechanical damage of the asperities in contact, the maximum value of normal stress applied on the fracture during the rematching was 10 MPa.

$$\sigma_v = \sigma_{v0} + 0.0255 \times (\text{depth} - 1377) \quad \text{with } \sigma_{v0} = 1377 \times 0.024 \quad [\text{MPa}] \tag{1}$$

For the test, the 70-mm-diameter cylindrical sample was re-cored perpendicular to the fracture such that the mean plane of the fracture was perpendicular to the cylinder axis. The height of the cylinder is 35 mm.

For this test, the temperature has been set to 100 °C. This value was arbitrarily selected lower than the in situ temperature submitted by the fracture at 1890 m (estimated more or less at 140 °C) in order to reduce the risk of evaporation of the fluid and salt crystallisation during the test.

All the maps (void thicknesses, wall topography, chemical elements) were obtained before the rock sample was placed in the experimental apparatus. The X-ray microfluorescent mapping of the chemical elements was done at CEREGE (Aix-en-Provence, France) on an XGT700 spectrometer. Taking into account that the surface of the fracture walls is not flat, the acceleration voltage of the electrons for the acquisition of the X-ray spectrum was set at 30 kV, which implies a characterisation of the elements to a depth of the order of one millimetre.

Mineralogical characterisation

Through visual descriptions using an optical microscope, the rock is granite porphyry with multicentimetre phenocrysts of pinkish potassium feldspar in a grey to greenish matrix of medium-size grains of quartz, plagioclase, potassium feldspar, biotite and metal oxides. The natural fracture shows signs of hydrothermal circulation. The fracture walls (Fig. 6) have a very thin coating, less than a millimetre thick, of evenly distributed calcite.

Based on these descriptions, the composition of the fluids, used during the characterisation phases of the fracture's hydromechanical behaviour, has been determined to be in equilibrium with the minerals of the rock sample especially with the calcite in order to avoid any dissolution of the coating on the fracture walls. For the temperature condition of the test (100 °C), the inert fluid was water with a calcium and bicarbonate concentration of $[Ca] = 2.1 \cdot 10^{-4}$ mol/L and $[HCO_3^-] = 2.4 \cdot 10^{-4}$ mol/L, respectively.

Morphological characterisation of the fracture

Initial wall topography The initial analysis of the fracture wall heights (Fig. 7) through statistics based on the entire wall surface areas shows a similar distribution for the lower and upper (inverted axes) wall heights (Fig. 8), although without these being statistically identical (χ^2 test at the 5 % significance level). The amplitudes of the intercentile heights (between the 0.01 and 0.99 percentiles) are 6.1 mm for the lower wall and 6.3 mm for the upper wall (see Fig. 9 for an example of two height profiles corresponding to the upper and lower walls). The height variations occur at different scales and break down into at least two wavelengths.

The topographic variations differ depending on the considered direction: they appear greater in the N0° direction (Fig. 7) than in the N90° direction. This anisotropy is quantified in terms of amplitude by calculating the linear roughness, defined as the ratio of the actual length of the profile to its projection on the reference line defined as the horizontal (line contained in the median plane). The average linear roughness is greater in the N0° direction (e.g. RL = 1.14 for the lower wall) than in the N90° direction (e.g. RL = 1.09 for the lower wall). This result is supported by the variographic study of the heights (see Fig. 10 for the lower wall before the reactive percolation) which shows a marked anisotropy of the surface characterised by different levels according to the directions of the variogram calculation: the variogram calculated in the N0° direction has

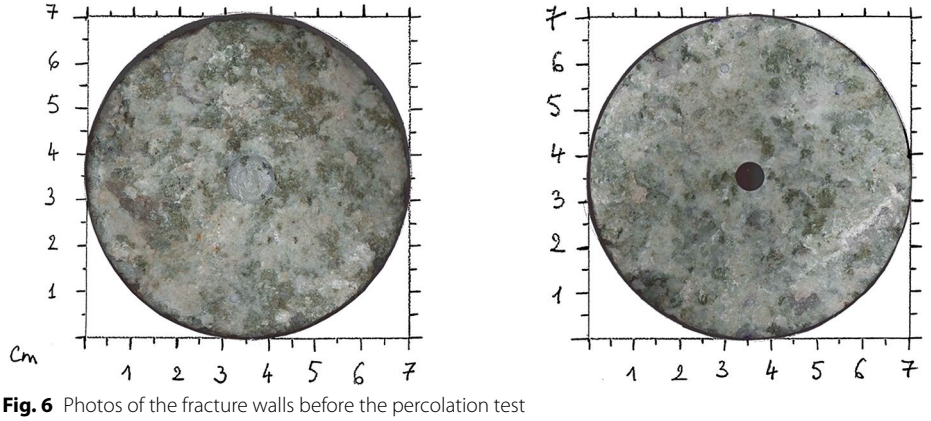

Fig. 6 Photos of the fracture walls before the percolation test

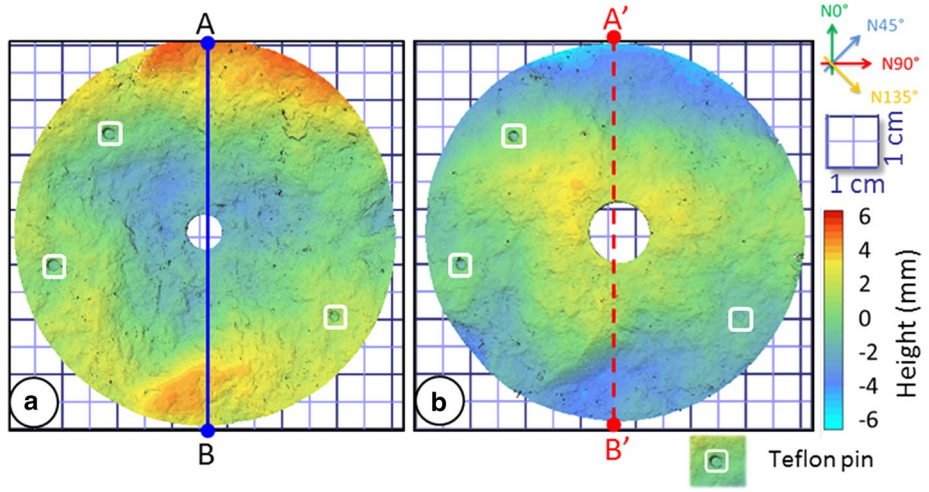

Fig. 7 Map of the lower (**a**) and upper (**b**) wall heights. AB and A'B': positions of Fig. 9 profiles

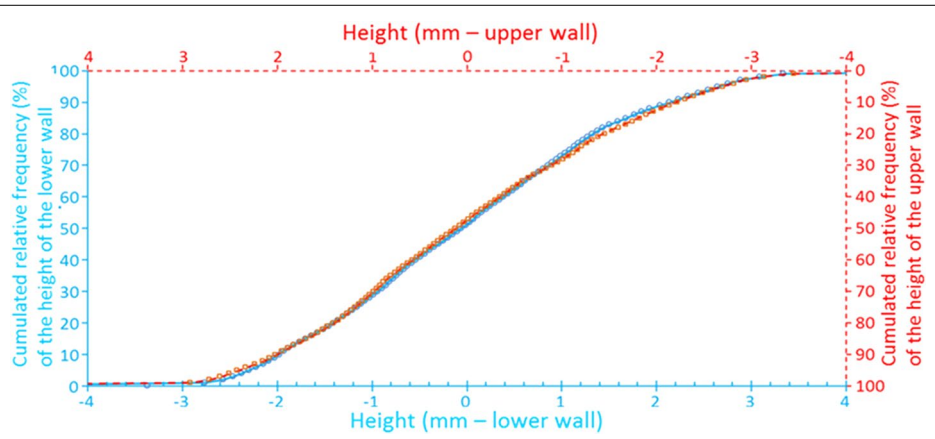

Fig. 8 Cumulative distribution of the lower (*blue*) and upper (*red*) wall heights

higher values than that calculated in the N90° direction, regardless of the distance considered. This anisotropy is a result of greater height variations in the N0° direction than in the N90° direction. The variograms can also be adjusted with cubic laws of different ranges, equal to 25 mm in the N90° direction and 30 mm in the N0° and N45° directions, denoting an anisotropy in the height variation frequency on a multicentimetre scale.

Map of the initial voids The average initial thickness of the voids between the fracture walls is 0.10 mm. The individual thicknesses, however, are very variable, characterised by a variation coefficient of 120 % (Fig. 11a). The void thickness distribution shows a long tail towards the high values. The void map (Fig. 11a) shows that the very thick voids form islands, some of which can be associated with the three pins used as reference points and with damage at the sample edge from the coring.

The variogram analyses of the void thicknesses (Fig. 11b) reveal spans of less than or equal to 5 mm for the four studied directions with no directional anisotropy.

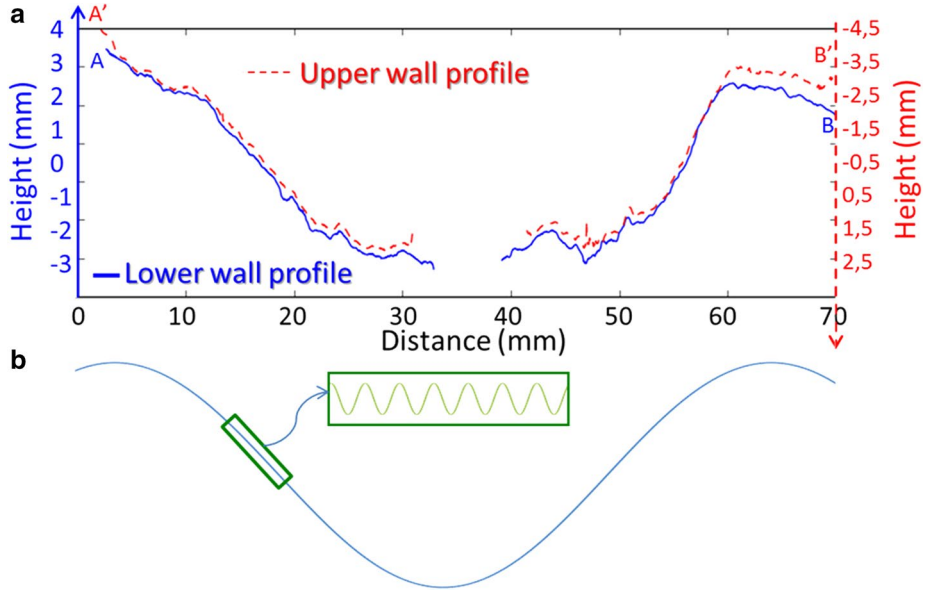

Fig. 9 Height profiles. Profiles AB and A'B' of the lower and upper walls (**a**) and simplification of the different height variation scales (**b**)

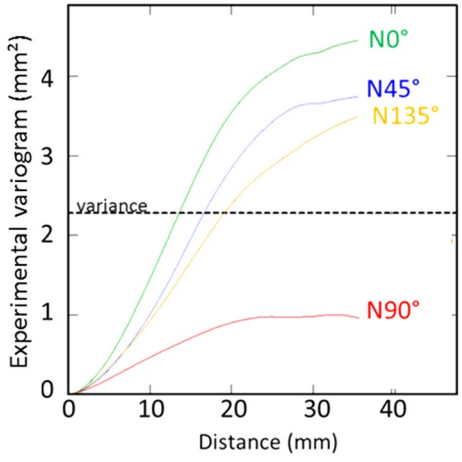

Fig. 10 Directional variograms of the lower wall heights

Interpretations of the fracture morphology The various observations and measurements made on the height and void maps have revealed height and void thickness variations with two distinct wavelengths.

Variations with multicentimetre wavelengths are seen both on the profiles of the height maps (Fig. 9b) and on the associated variograms (Fig. 10), but were not detected on the void maps. These lengths are probably associated with the fracture mechanics at the onset of rupture; the topographies of the two walls are thus very similar (matching walls). Furthermore, one finds an anisotropy on the height variograms probably related to the origin of these structures.

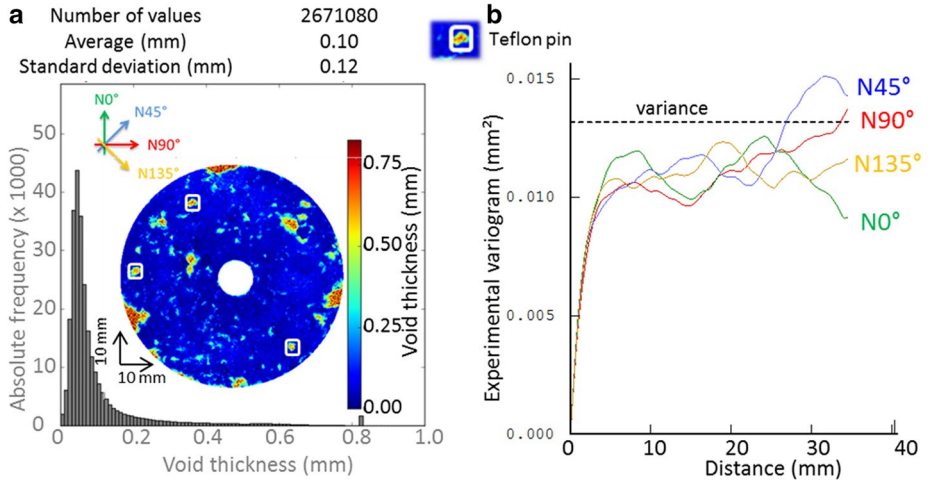

Fig. 11 Void thicknesses analysis. Map and distribution of the void thicknesses (**a**); directional variograms of the void thicknesses (**b**)

A second, millimetre-sized, wavelength range is seen both on the height profiles (Fig. 9b) and on the void thickness variograms (Fig. 11b). These shorter wavelengths, probably initially structured by the fracture mechanics, correspond to a scale showing variations from one wall to another. They reflect local developments in the fracture probably due to precipitation and dissolution resulting from hydrothermal circulation. No anisotropy has been demonstrated, which tends to show a tendency for a non-favoured flow in a given direction, and may corroborate the observation determined from the walls that no indications of shear are observed.

Initial mechanical behaviour of the fracture under normal stress

Once the sample was installed in the experimental apparatus and the fracture rematched, a test was carried out to characterise the fracture's mechanical behaviour under normal stress and temperature (100 °C set as the heating resistor temperature). Increasing levels of normal stress (2.6, 4.9, 7.2 and 9.4 MPa) were applied to the fractured sample in order to measure the mechanical response from the displacement sensors. Figure 12[1] shows the displacement increments measured by the four LVDT sensors as a function of the normal stress applied to the sample. This evolution, within the applied normal stress range, is just about linear without any pronounced non-linearities. The average displacement increment was of the order of 0.03 mm for a normal stress of 9.4 MPa. Considering a Young's modulus of 38 GPa for the Soultz granite (Rummel 1991), the axial elastic contraction of a rock cylinder of 35 mm height is more or less than 0.007 mm for an increase of normal stress from 2.6 to 9.4 MPa. As a first approximation, the comparison with the displacement increment measured enables us to disregard the deformation of the walls themselves and to consider that the relative displacements measured between the walls corresponded to the opening or closing of the fracture.

[1] Because of fluctuations in certain control elements of the experimental apparatus (e.g. regulation of the confining cell pressure, the normal stress application, the test room temperature) and because of the complexity of their interactions and their impact on the measured parameters, no error calculations have been made concerning the data presented in this article.

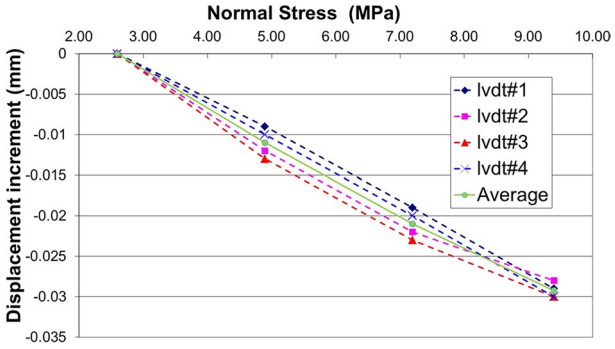

Fig. 12 Evolution of the relative displacements between the walls under normal stress before the percolation test

Initial hydraulic behaviour of the fracture under normal stress

In order to characterise the hydraulic response of the fracture under normal stress and temperature, injection tests were carried out for each of the normal stress levels by measuring the injection pressure for different imposed injection flow rates. For each injection test, the displacements were checked to ensure that they remained constant and the induced fluid pressure did not change the fracture aperture. Figure 13 shows the evolution of injection pressure as a function of the imposed injection flow rate. It was found that the fracture's hydraulic response was highly dependent on the normal stress level, with four very distinct trends in injection pressure versus flow. For a given injection rate, the injection pressure increased as the normal stress increased; thus for a flow rate of 30 ml/h, the injection pressure was 0.3 MPa under 2.6 MPa of normal stress and reached 3 MPa under 9.4 MPa of normal stress. Where the fracture's flow regime is concerned, the evolution of injection pressure with injection rate was linear for the lowest normal stress level (2.6 MPa), corresponding to a laminar flow regime. For higher normal stress levels (4.9, 7.2 and 9.4 MPa), it seems that the curves show some inflection points and it is more difficult to decide on the linearity of the hydraulic response. At first approximation, in order to estimate the flow regime in the fracture using the Reynolds number, Karbala et al. (2009) assume that the hydraulic diameter corresponds to two

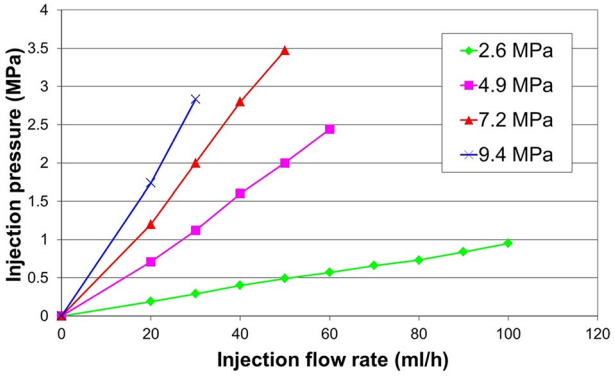

Fig. 13 Evolution of injection pressure as a function of injection flow rate under different normal stress levels before the percolation test

times the hydraulic aperture for a radial flow between two parallel smooth disc planes. Based on this, the Reynolds number could be expressed by

$$\mathrm{Re} = \rho Q/(\pi \eta \mathrm{r}), \tag{2}$$

where ρ and η are the density (10^3 kg/m^3) and the dynamic viscosity ($2.\cdot10^{-4}$ Pa.s) of the fluid, respectively, Q the injection flow rate and r the considered radius. Considering the radius at the injection point in the fracture ($r = 5.6\cdot10^{-3}$ m) and a Reynolds number of 2100, being the upper limit for laminar flows, the critical injection flow rate is evaluated to be 26,000 ml/h. Even if the assumptions made for this calculation are very strong considering flow in natural non-smooth fractures, one can assume that the levels of injection flow rate are far from this critical value and thus the fluid flow in the fracture will be globally laminar.

Reactive percolation test

A synthetic brine was injected for the reactive percolation test; its chemical composition (Table 1) was defined on the basis of the in situ fluid at the Soultz-sous-Forêts site, but with a lower concentration of certain elements so as to limit the risk of secondary mineral phases precipitating and clogging the tubes for evacuating the fluid after its circulation in the fracture. The injection rate and normal stress conditions chosen for this test were based on the previously determined hydromechanical characterisations so as to ensure, as far as possible, a laminar flow regime throughout the test; the injection rate was set at 30 ml/h and the normal stress at 1.35 MPa. It should be noted that the normal stress was initially set at 1.9 MPa, but following a sharp increase in injection pressure during the first hour of the test (point A in Fig. 17), it was lowered to 1.35 MPa for the remainder of the test. The heating resistor temperature was fixed at 100 °C which, under the test conditions, corresponded to a temperature of 85 °C at the point of injection into the fracture. The reactive test was conducted over 17 days, ensuring that the conservation criterion of the amount of fluid exiting the chamber, set at 10 percent, was well respected.

Table 1 Chemical composition of the synthetic brine

Elements	Concentration [mol/L]
Al	$9.64\cdot10^{-8}$
SiO_2	$3.28\cdot10^{-5}$
Mg	$6.01\cdot10^{-3}$
Fe	$9.13\cdot10^{-7}$
Cl	$1.53\cdot10^{0}$
HCO_3	$1.42\cdot10^{-5}$
Ba	$6.92\cdot10^{-6}$
Ca	$1.03\cdot10^{-1}$
K	$7.93\cdot10^{-2}$
Na	$1.22\cdot10^{0}$
Sr	$5.39\cdot10^{-3}$
SO_4	$2.08\cdot10^{-3}$

Figure 14 shows the evolution of the injection pressure throughout the 17 days of the test. Two phases can be distinguished: a phase termed reactive during the first 3 days (4320 min) and then, after 7 days of the test (or 10,080 min) indicated by point B in Fig. 14, a phase of injection pressure stabilisation at around a value of 0.15 MPa. Problems of regulating the normal stress between these two phases (see Fig. 14) resulted in an increase in the injection pressure that is consequently difficult to tie in with the physicochemical changes induced by the fluid–rock interactions.

The evolution of the physicochemical parameters, measured online throughout the test, seems to show a similar trend to that of the injection pressure: a first phase during the first days of the test showing the strongest changes, followed by a phase of parameter stabilisation. The evolution of pH (Fig. 15) shows a progressive decline from a value of 8.2, which was the value of the initial pH of the injected fluid, to stabilise after the first 7 days of the test (point B in the figure) at around pH 7.5. The Eh (Fig. 16) shows a decline to a plateau around −110 mV at the beginning of the test, then a gradual rise to reach a stabilisation level, also after the first 7 days of the test (point B in the figure), around an Eh of 25 mV. In order to explain quantitatively these pH and Eh evolutions, a detailed chemical analysis is required by considering the whole series of possible

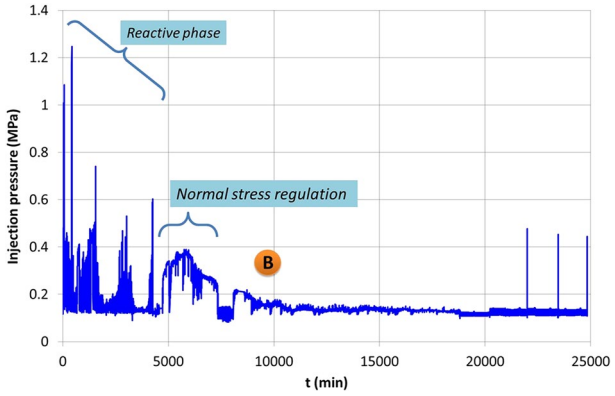

Fig. 14 Evolution of the injection pressure during the 17-day reactive percolation test

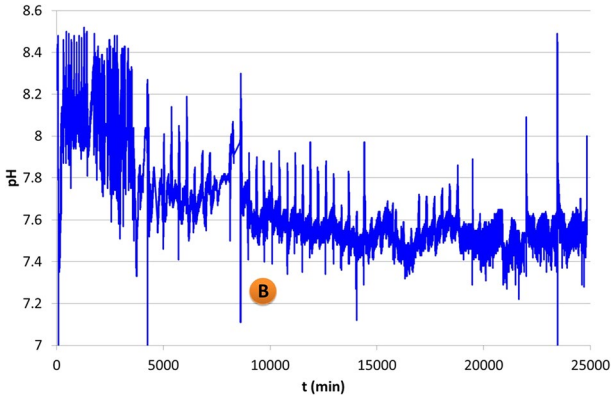

Fig. 15 Evolution of the pH during the 17-day reactive percolation test

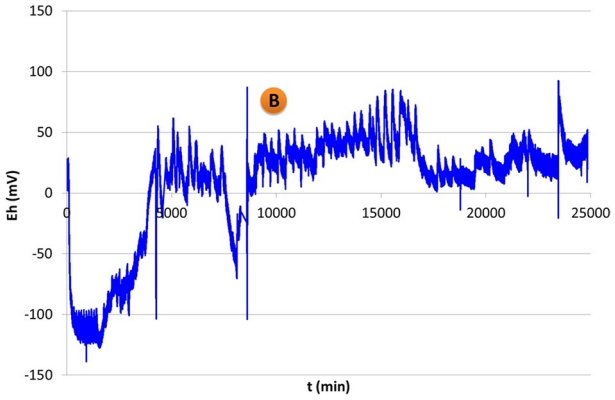

Fig. 16 Evolution of the Eh during the 17-day reactive percolation test

reactions with the minerals of the rock sample and the chemical elements in the fluid. This is not presented in the framework of this article.

From the 17-day evolution of the injection pressure, pH and Eh, it appears that the major changes occurred during the first phase of the test, named "reactive" in Fig. 14. Looking at this reactive phase in more detail, Fig. 17 gives the evolution of the injection pressure over these first 3 days of the test. It shows that the injection pressure progressively increased to more than 1 MPa during the first hour. To avoid any risk of pressure build-up that could lead to a hydraulic fracturing of the sample (especially at the level of the hole drilled in the lower wall to inject the fluid), the normal stress level was reduced from 1.9 to 1.35 MPa, resulting in an immediate fall in the injection pressure (point A in Fig. 17). The injection pressure then followed a regular sawtooth evolution (highlighted by the red dashed line in Fig. 17) showing a succession of increase/decrease phases punctuated, after the first day of the test, by stages during which the injection pressure was relatively stable. These increase/decrease phases of the injection pressure indicate a succession of decreases and increases of the overall fracture permeability, and are apparently not connected to the fracture's openings and closings. In fact, over the same test period, the evolution of the relative wall displacements (Fig. 18) has a different

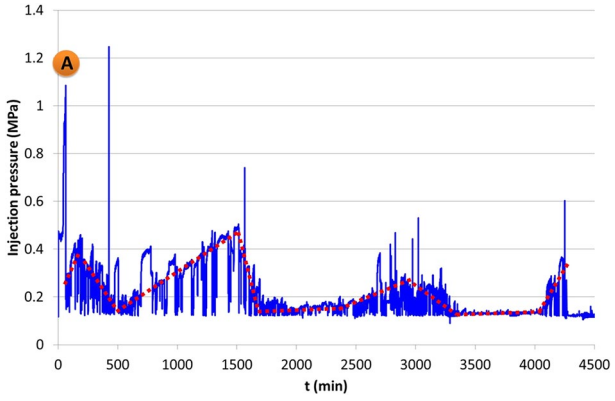

Fig. 17 Evolution of the injection pressure during the first 3 days of the reactive percolation test

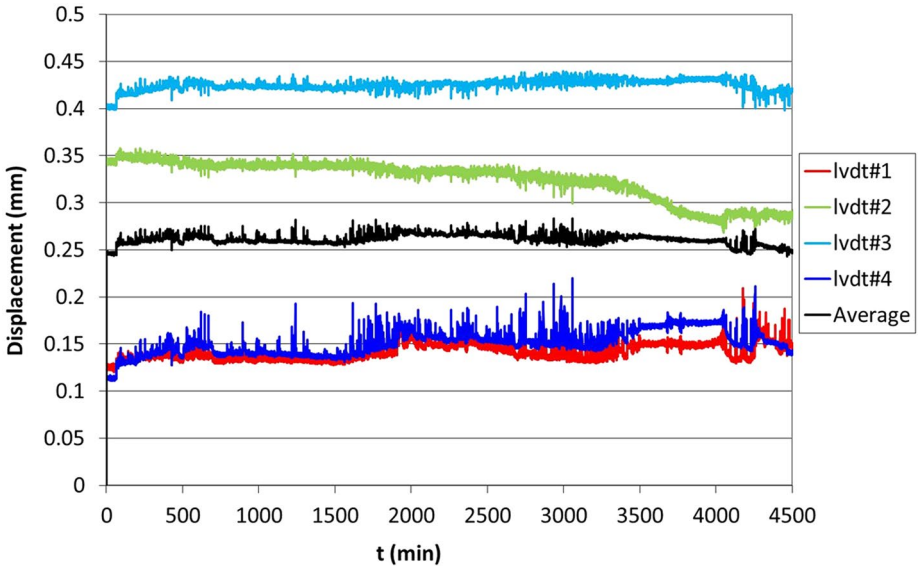

Fig. 18 Evolution of the relative wall displacements during the first 3 days of the reactive percolation test

appearance to that of the injection pressure. It is thus likely that the permeability fluctuations are related to chemical interactions between the fluid and the fracture, such as a series of precipitations/dissolutions, influencing the flow within the latter.

In addition to the physical and chemical changes being measured during the test, fluid samples were taken in order to analyse the changes in the chemical composition of the fluid following its percolation through the fracture. The concentrations of most of the chemical elements (major cations Na, K, Ca, Mg, Sr, silicon and aluminium ions, anions, trace elements) were analysed. All the analysed samples showed a bicarbonate (HCO_3^-) supersaturation (Fig. 19), whereas the concentration of the injected fluid was undersaturated vis-à-vis calcite, thus indicating a dissolution of calcite throughout the test.

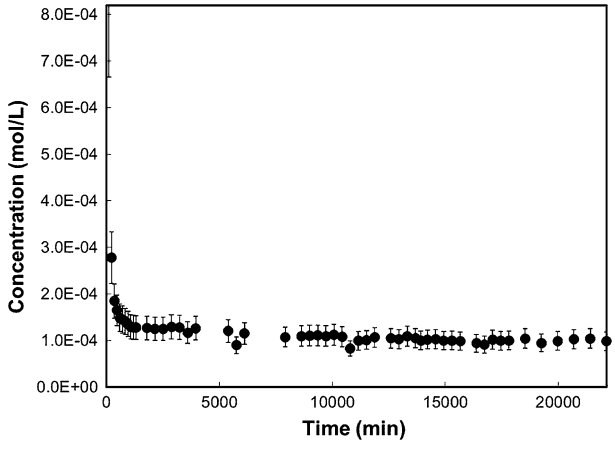

Fig. 19 Evolution of the bicarbonate HCO_3^- concentration of the collected fluid samples with respect to time

Changes induced by the reactive percolation

Mineralogical evolution of the fracture walls

Observation of the fracture walls under the binocular microscope after the test showed mainly dissolution of the calcite coating. Dissolution also affected some of the granite's primary minerals: the biotite and plagioclase are rounded, highlighted and more exposed. The potassium feldspar and quartz, as such, were not affected by the dissolution and do not seem to have reacted significantly with the injected fluid.

The X-ray microfluorescent mapping of the chemical elements only locally corroborates these observations because the analytical parameters chosen for the acquisition of the X-ray spectrum for this test involved characterising the elements to a depth of the order of a millimetre. This is limiting for capturing the changes due to phenomena whose depth of influence is less than a millimetre, such as the dissolution of the calcite film whose thickness was initially less than a millimetre. However, the X-ray microfluorescent mapping of the calcium did locally enable the observed dissolution of calcite to be corroborated. Figure 20 shows the lower wall calcium maps before and after the percolation test. These would appear to show (Fig. 20b) that in a confined region around the injection point (delimited by the dotted circles) the calcium has disappeared from certain areas, which may attest locally to the dissolution of calcite.

Evolution of the fracture morphology

Evolution of the wall topographies Overall, the morphology of surfaces showed no, or only slight, changes after the test; the differences noted between the linear roughness and the variograms before and after the test fall within the measurement error. If changes did occur, they would have been local modifications that the global parameters could not bring to light.

The asperity height difference maps of the walls before and after the percolation test (Fig. 21) are particularly noisy due to the difficulty in superposing the maps; nevertheless, two areas, denoted α and β, appear to show height differences over a relatively wide area. However, due to the error associated with the measurement and the repositioning

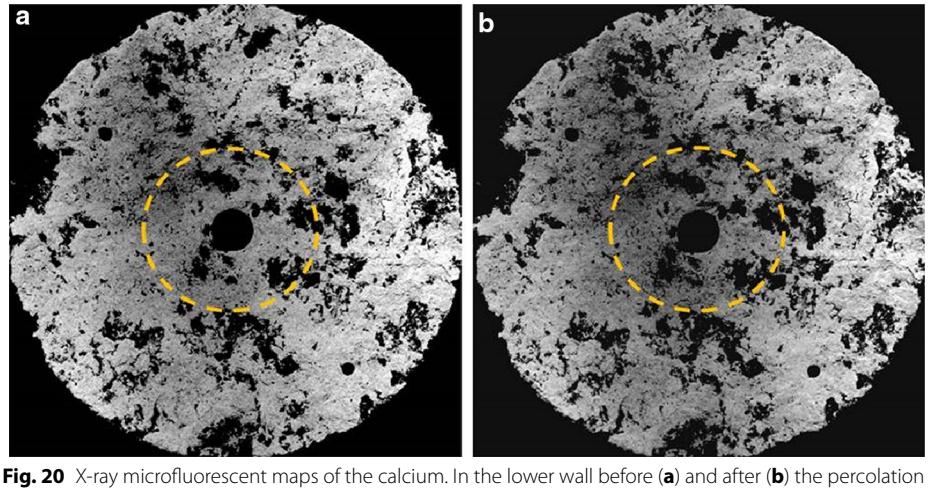

Fig. 20 X-ray microfluorescent maps of the calcium. In the lower wall before (**a**) and after (**b**) the percolation test (*black* shows the absence of calcium)

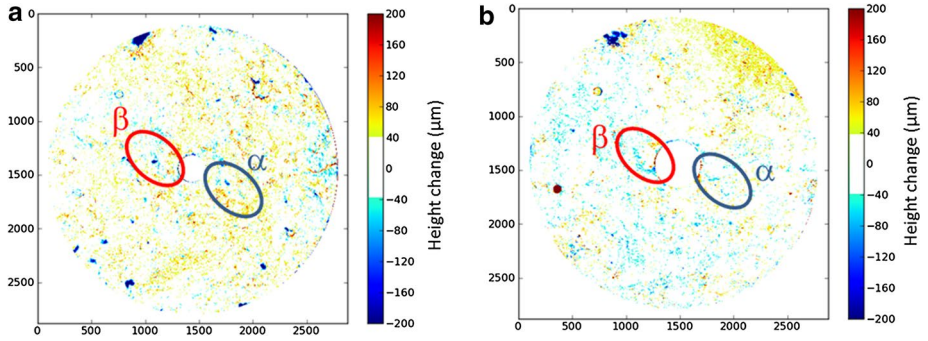

Fig. 21 Evolution of the granite sample's fracture morphology. Height differences before and after the test (negative values: material loss) for the lower (**a**) and upper (**b**) walls

of the walls, it is not possible to conclude on these local observations of modification in the surface morphologies.

Evolution of the fracture's void thicknesses Geostatistical analyses were carried out to quantify possible global changes in the void thicknesses. In particular, variographic analyses on increasingly large doughnut-shaped patches centred on the injection zone were carried out to determine the distance to which any changes linked to the action of the injected fluid could be measured.

The void thickness variograms calculated on the subcentimetre-thick corona show a higher stage after the percolation than those calculated on the initial data. This indicates that variations in void thickness in a subcentimetre area around the injection zone are greater after the percolation test than before. Figure 22 shows the void thickness difference map thresholded to meaningful values based on the error calculations performed on the maps before and after the reactive percolation. On this map, one can see localised thickness increases on relatively narrow surfaces. However, these may be the result of unquantified errors in recalibrating the maps before and after the reactive percolation,

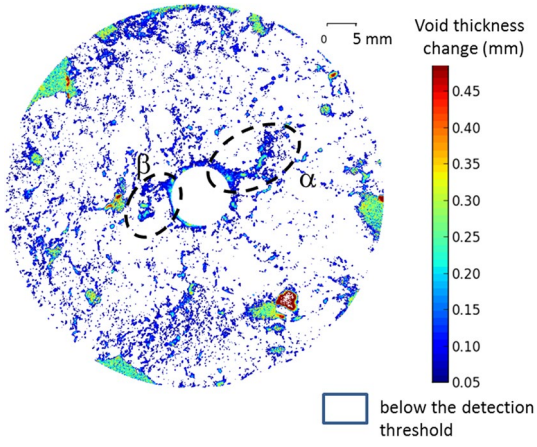

Fig. 22 Void thickness difference map of the fracture. The map is obtained by subtracting the map of initial void thicknesses from that plotted after the test

and will not be considered except for areas where the increase in void thickness forms channels of more than a millimetre width (α and β, Fig. 22). The route of these channels extends for a distance of up to 8 mm from the injection chamber; their location corresponds to that of the observed changes in the wall topographies (Fig. 21). As can be seen in Fig. 23, the increase in void thickness is far greater than the errors associated with the measurement and recalibration.

Evolution of the fracture's mechanical behaviour

The loading protocol under normal stress used during the initial characterisation was again followed after the percolation test in order to characterise the fracture's mechanical behaviour. Figure 24 shows the evolution of the relative displacements between the two fracture walls, as measured by the LVDT sensors, with normal stress applied to the rock sample. The curves show a slight inflection point for the first loading increment at 4.9 MPa, particularly with displacement sensors LVDT #3 and #4. The closures under this normal stress level are slightly greater (of the order of −0.013 mm on average) than in the initial characterisation (see Fig. 12: average closure of the order of −0.011 mm). With the following normal stress increments, the closures are comparable to those measured before the reactive percolation test, with the average closure being of the order of −0.03 mm at 9.4 MPa. It therefore appears that, apart from the first normal

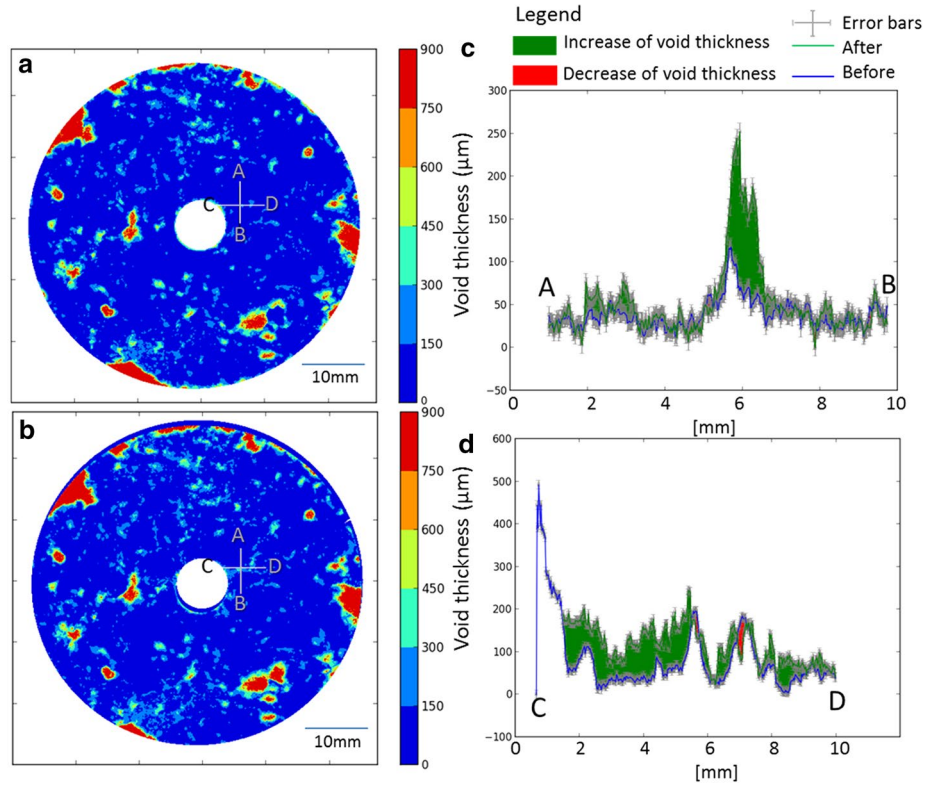

Fig. 23 Maps of the void thicknesses. Before (**a**) and after (**b**) the percolation test and location of the AB and CD sections; (**c**) and (**d**) profiles of the void thicknesses, before and after the percolation test, along sections AB and CD intersecting the channel of the defined zone α in Fig. 22

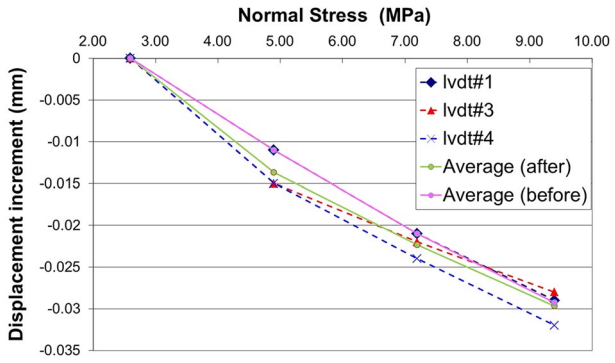

Fig. 24 Evolution of the relative displacements in the walls under normal stress after the percolation test. For comparison, both average evolutions, before and after the percolation test, are drawn. The sensor LVDT #2 was blocked during the reactive test

stress increment, the overall mechanical behaviour of the fracture was only slightly modified by the reactive percolation test.

Evolution of the fracture's hydraulic behaviour under normal stress

As with the mechanical behaviour, the hydraulic behaviour tests made after the reactive percolation were identical to those made before, with a hydraulic test being carried out for each normal stress level. Figure 25 shows the evolution of the injection pressure measured at the centre of the fracture as a function of the imposed flow rate for the different stress levels. First, it should be noted that, for the same normal stress levels, the range of imposed flow rates is here greater (up to 200 ml/h) than during the tests performed before the percolation (up to 100 ml/h), while at the same time the range of the measured injection pressures is smaller (less than 1.2 MPa here, as opposed to less than 3.5 MPa before). This observation indicates a general increase in the fracture's permeability induced by the reactive percolation. As regards the influence of the normal stress on the hydraulic behaviour, the evolution of the injection pressure with injection flow rate is very similar for the three highest stress levels (4.9, 7.2 and 9.4 MPa); thus, it appears that the mechanical loading has a moderate influence on the hydraulic behaviour.

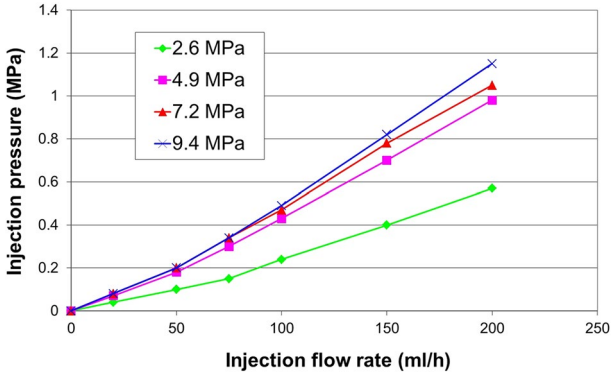

Fig. 25 Evolution of the injection pressure as a function of injection flow rate under different normal stress levels after the percolation test

Assuming that the flow in the fracture is isothermal, divergent radial and laminar between two smooth disc planes, a simplification of Navier–Stokes law makes it possible to calculate (Eq. 3) the fracture's intrinsic transmissivity, $k_f.e$. Notwithstanding the assumptions and limitations of this analytical solution, discussed notably by Karbala et al. (2009), calculation of the fracture's intrinsic transmissivity gives access to a global macroscopic parameter at fracture scale for characterising the fracture permeability and its evolution as a function of the mechanical loading.

$$k_f.e = -(\eta/2\pi)\,(Q/\Delta P)\,\mathrm{Ln}\,(\mathrm{Ri}/\mathrm{Re}), \tag{3}$$

where η is the dynamic viscosity of the fluid (Pa.s), Q is the volumetric flow rate (m^3/s), ΔP is the pressure difference (Pa) between the centre of the fracture (injection point) and its periphery (at containment cell pressure), Ri and Re (in m) are, respectively, the inner radius (radius of the injection well, $5.6{\cdot}10^{-3}$ m) and the outer radius (radius of the rock sample $35{\cdot}10^{-3}$ m).

Figure 26 shows the evolution of the intrinsic transmissivity (for an injection flow rate of 50 ml/h) as a function of the normal stress both before and after the reactive percolation test; two differences can be seen between the two evolutions, the one on the range of values and the other on the influence of the normal stress. In the first instance, the intrinsic transmissivity values are higher after the reactive percolation, indicating an increase in the fracture's permeability; this increase is approximately one order of magnitude at normal stress level. Secondly, the shape of the evolutions under the applied normal stress is different; before the reactive percolation test, the intrinsic transmissivity decreased continuously under the normal stress, whereas after the test it decreased during the first normal stress levels before stabilising at a value of $1.4{\cdot}10^{-14}$ m^3 as of the 7.2 MPa level.

Summary and interpretation of the test

The evolution of the parameters, such as injection pressure and pH, in the reactive percolation test shows a period of physical–chemical reactivity concentrated mainly in the first 7 days of the test, followed by a period of stabilisation.

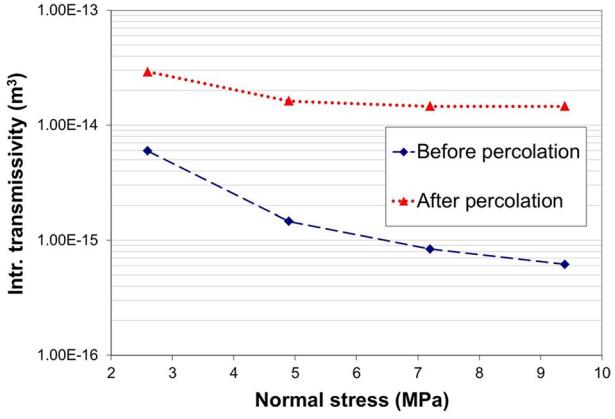

Fig. 26 Evolution of the fracture's intrinsic transmissivity (in logarithmic scale) as a function of the normal stress before and after the reactive percolation test

All the physical characterisations and tests carried out on the fracture before and after the reactive percolation highlight the changes induced by the percolation:

- visual observation of the fracture walls showed mainly a dissolution of the calcite coating, as well as dissolution of the plagioclase, locally very rounded, and an alteration of the biotite;
- the morphological characterisation (fracture void map and wall topography map) shows the formation of "channels", more than a millimetre depth, starting from the injection zone and winding away up to a distance of 8 mm;
- the fracture's mechanical behaviour under normal stress was hardly affected by the chemical interactions;
- the reactive percolation decreased the impact of mechanical loading on the fracture's hydraulic behaviour;
- the fracture's intrinsic transmissivity decreased by an order of magnitude due to the reactive percolation.

Based on the above points, a coherent explanation of the increase in the fracture's permeability (highlighted by the evolution of the intrinsic transmissivity) is that the fluid/rock interaction led to a deepening of existing channels, this being fairly pronounced immediately around the injection point, without having affected the contact points that govern the fracture's mechanical behaviour. Figure 27 schematically represents this hypothesis. It would therefore appear from this test that the dissolution phenomena (dissolution of the calcite, plagioclase) are rather of the *free face dissolution* type and that the *pressure solution* phenomena described by some authors (e.g. Polak et al. 2003; Yasuhara et al. 2006) were limited. With the occurrence of the latter being related to the

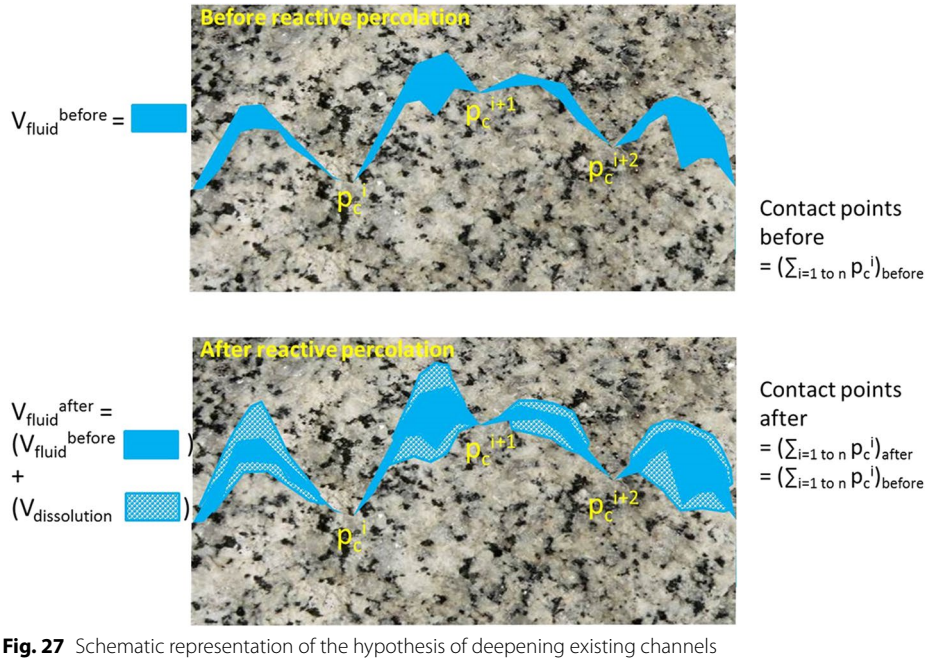

Fig. 27 Schematic representation of the hypothesis of deepening existing channels

mechanical loading and effective stress applied to the fracture (McGuire et al. 2013), the announced findings from the present test should be placed in a specific context linking 'sample'-'injected fluid' along with the test conditions (mechanical loading, injection pressure, temperature, etc.).

Conclusions and outlook

The reactive percolation tests in a fracture under THM conditions are aimed at improving our understanding of fluid/rock interactions and their influence on fracture flow. To achieve this objective, the developments described here were focused not only on the use of a specially designed experimental apparatus but also on an associated test methodology. The system makes it possible to carry out a reactive percolation test as such, as well as characterise the changes induced by the fluid/rock interactions. These changes are characterised both at the overall fracture scale, as regards its mechanical and hydraulic behaviour, and at microscopic scale through mapping the morphology and mineralogy of the fracture walls and also the voids. Combining all the data and characterisations obtained during the test enables one to draw up scenarios linking the nature of the fluid/rock interactions produced during the reactive test, their effect on the physical characterisation of the fracture (morphology, voids map, minerals) and the evolution of the resulting macroscopic behaviour (hydraulic and mechanical).

To illustrate this, we have described a percolation test conducted on a sample of fractured granite (natural fracture showing signs of hydrothermal circulation). The test showed that the *free face type dissolution* of some minerals led, through a deepening of existing channels on the fracture walls, to an increase of the fracture's permeability by one order of magnitude and to a change in its hydromechanical behaviour.

The results obtained during these tests under certain THM conditions are of vital interest for evaluating the evolution of fracture permeability during the development phase of an EGS reservoir. In addition to these experimental studies, modelling is being carried out to deepen and extrapolate the results and observed behaviours under certain THM conditions. The path being followed is one of the models based on geometric construction using the fracture's morphological data, thus making the most of the different maps produced during the experimental tests. Coupled models reproducing the fracture's contact points, as has been done by Ameli et al. (2014), can reproduce the evolution of the flow within the fracture as a function of applied normal stress whilst incorporating evolution laws of the contact points to reproduce the fluid/rock interactions. More generally, in order to transpose the impact of the permeability changes observed at the single fracture scale to an EGS reservoir scale, the results need to be interpolated and integrated within reservoir scale models (Taron and Elsworth 2010; Pandey et al. 2014; Huang et al. 2014).

Authors' contributions

AB carried out the experimental tests and their analyses, and drafted the manuscript. MP carried out the morphological analyses of the fracture and wrote the concerned parts of the manuscript. SG initiated these experimental tests 15 years ago and brang her skills and expertise in rock fracture behavior. All authors read and approved the final manuscript.

Acknowledgements

This work was co-financed by the French Environment and Energy Management Agency (ADEME).
The authors would especially like to thank Christophe Poinclou (ANTEA) for his help and generous technical support during the development and application of the experimental apparatus.

Competing interests
The authors declare that they have no competing interests.

Received: 28 September 2015 Accepted: 11 January 2016
Published online: 23 January 2016

References

Ameli P, Elkhoury JE, Morris JP, Detwiler RL. Fracture permeability alteration due to chemical and mechanical processes: a coupled high-resolution model. Rock Mech Rock Eng. 2014;47:1563–73. doi:10.1007/s00603-014-0575-z.
Bandis SC, Lumsden AC, Barton NR. Fundamental soft rock joint deformation. Int J Rock Mech Min Sci. 1983;20(6):249–68.
Barton N, Choubey V. The shear strength of rock joints in theory and practice. Rock Mechanics. 1977;10:1–54.
Barton N, Makurat A. Hydro-thermo-mechanical over-closure of joints and rock masses and potential effects on the long term performance of nuclear waste repositories. In: Cotthem, Charlier, Thimus, Tshibangu, editors. Proceedings of Eurock2006 Multiphysics coupling and long term behavior in rock mechanics, Liege; 2006. p. 445–50.
Brown S, Scholz C. Closure of rock joints. J Geophys Res. 1986;91(B5):4939–48.
Cornet FH, Bérard T, Bourouis S. How close to failure is a granite rock at a 5 km depth? Int J Rock Mech Min Sci. 2007;44:47–66.
Crandall D, Bromhal G, Karpyn ZT. Numerical simulations examining the relationship between wall-roughness and fluid flow in rock fractures. Int J Rock Mech Min Sci. 2010;47:784–96.
Chilès JP, Gentier S. Geostatistical modelling of a single fracture. In: Soares A, editor. Geostatistics Troia '92. Dordrecht: Kluwer Academic Publishers; 1993. p. 95–108.
Duncan N, Hancock KE. The concept of contact stress 10 assessment of the behavior of rock masses as structural foundations. Proc First Cong. Int. Soc. Rock Mech. Lisbon 2; 1966. p.487–492.
Gale JE. Comparison of coupled fracture deformation and fluid models with direct measurements of fracture pore structure and stress-flow properties. In: Farmer IW, Daemen JJK, Desai CS, Glass CE, Neuman SP, editors. Rock mechanics: proceedings of the 28th US Symposium. Tucson, Arizona. Rotterdam: Balkema; 1987. p. 1213–22.
Ge Y, Kulatilake PHSW, Tang H, Xiong C. Investigation of natural rock joint roughness. Comput Geotech. 2014;55:290–305.
Genter A, Evans KF, Cuenot N, Fritsch D, Sanjuan B. Contribution of the exploration of deep crystalline fractured reservoir of Soultz to the knowledge of Enhanced Geothermal Systems (EGS). Geoscience. 2010;342:502–16.
Gentier S, Billaux D. Caractérisation en laboratoire de l'espace fissural d'une fracture. In: Maury V, Fourmaintreaux D, editors. Rock at great depth, Pau, France. Rotterdam: Balkema; 1989. p. 425–31.
Gentier S, Billaux D, Van Vliet L. Laboratory testing of the voids of a fracture. Rock Mech Rock Eng. 1989;22:149–57.
Gentier S, Baranger P, Bertrand L, Rouvreau L, Riss J. Chemical interaction between rock and fluid in a fracture : experimental approach. In: "3D modeling, time dependence and complex interaction", 3rd international conference on mechanics of jointed and faulted rock (MJFR-3), Vienna; 1998, p 589–594.
Gentier S, Riss J, Archambault G, Flamand R, Hopkins D. Influence of fracture geometry on shear behavior. Int J Rock Mech Min Sci. 2000;37:161–74.
Hopkins DL. The implications of joint deformation in analyzing the properties and behavior of fractured rock masses, underground excavations, and faults. Int J Rock Mech Min Sci. 2000;37:175–202.
Huang Y, Zhou Z, Wang J, Dou Z. Simulation of groundwater flow in fractured rocks using a coupled model based on the method of domain decomposition. Environ Earth Sci. 2014;72:2765–77. doi:10.1007/s12665-014-3184-y.
Iwai K. 1976, Fundamental studies of fluid flow through a single fracture.PhD thesis. Berkeley: University of California.
Karbala M, Katibeh H, Sharifzadeh M. Numerical and analytical hydraulic characterization of a horizontal single joint based on radial flow in water pressure test. J Appl Sci. 2009;9(10):1859–69 **(ISSN 1812–5654)**.
Keller A. High resolution, non-destructive measurement and characterization of fracture apertures. Int J Rock Mech Min Sci. 1998;35(8):1037–50.
Maerz NH, Franklin JA, Bennett CP. Joint roughness measurement using shadow profilometry. Int J Rock Mech Min Sci Geomech Abstr. 1990;27(5):329–43.
Matsuki K, Wang EQ, Sakaguchi K, Okumura K. Time-dependent closure of a fracture with rough surfaces under constant normal stress. Int J Rock Mech Min Sci. 2001;38:607–19.
McGuire TP, Elsworth D, Karcz Z. Experimental measurements of stress and chemical controls on the evolution of fracture permeability. Transp Porous Med. 2013;98:15–34.
MIT (Massachusetts Institute of Technology) Tester, Jefferson W. et al. The Future of Geothermal Energy—Impact of Enhanced Geothermal Systems (EGS) on the United States in the 21st Century. An assessment by an MIT-led interdisciplinary panel. Idaho Falls: Idaho National Laboratory; 2006. ISBN 0-615-13438-6. Retrieved 2007-02-07.
Pandey SN, Chaudhuri A, Kelkar S, Sandeep VR, Rajaram H. Investigation of permeability alteration of fractured limestone reservoir due to geothermal heat extraction using three-dimensional thermo-hydro-chemical (THC) model. Geothermics. 2014;51:46–62.
Polak A, Elsworth D, Yasuhara H, Grader AS, Halleck PM. Permeability reduction of a fracture under net dissolution by hydrothermal fluids. Geophys Res Lett. 2003;30(20):2020. doi:10.1029/2003GL017575.
Power CM, Hencher SR. A New Experimental Method For the Study of Real Area of Contact Between Joint Walls During Shear. In: Hassani, Mitri, editors. Rock Mechanics, Aubertin. Rotterdam: Balkema; 1996. ISBN 90 5410 838 X.
Pyrak-Nolte LJ, Myer LR, Cook NGW, Witherspoon PA. Hydraulic and mechanical properties of natural fractures in low permeability rock. In: Proceedings of the 6th congress international society for rock mechanics. vol. 1, Montreal; 1987. p. 225–31.
Re F, Scavia C. Determination of contact areas in rock joints by X-ray computer tomography. Int J Rock Mech Min Sci. 1999;36:883–90.
Rummel F. Physical rock properties of borehole GPK1. Geotherm Sci Tech. 1991;3:199–216.

Rutqvist J, Stephansson O. The role of hydromechanical coupling in fractured rock engineering. Hydrogeol J. 2003;11:7–40.
Taron J, Elsworth D. Coupled mechanical and chemical processes in engineered geothermal reservoirs with dynamic permeability. Int J Rock Mech Min Sci. 2010;47:1339–48.
Teufel LW, Logan JM. Effect of displacement rate on the real area of contact and temperatures generated during frictional sliding of Tennessee sandstone. Pure appl Geophys. 1978;116:840–65.
Yasuhara H, Polak A, Mitani Y, Grader AS, Halleck PM, Elsworth D. Evolution of fracture permeability through fluid-rock reaction under hydrothermal conditions. Earth Planet Sci Lett. 2006;244:186–200.
Yasuhara H, Elsworth D. Compaction of a rock fracture moderated by competing roles of stress corrosion and pressure solution. Pure Appl Geophys. 2008;165:1289–306.
Zhao Z, Liu L, Neretnieks I, Jing L. Solute transport in a single fracture with time-dependent aperture due to chemically medicated changes. Int J Rock Mech Min Sci. 2014;66:69–75.